ADVANCES IN ATMOSPHERIC SCIENCES, VOL. 39, JULY 2022, 1034–1049

• **Original Paper** •

# Seasonal and Diurnal Variations of Cloud Systems over the Eastern Tibetan Plateau and East China: A Cloud-resolving Model Study※

Jinghua CHEN*[1,2], Xiaoqing WU[3], Chunsong LU[1], and Yan YIN[1]

[1]*Collaborative Innovation Center on Forecast and Evaluation of Meteorological Disasters*, *Nanjing University of Information Science & Technology*, *Nanjing* 210044, *China*

[2]*Key Laboratory of Meteorology and Ecological Environment of Hebei Province*, *Shijiazhuang* 050022, *China*

[3]*Department of Geological and Atmospheric Sciences*, *Iowa State University*, *Ames*, *Iowa* 50011, *USA*

(Received 25 November 2020; revised 11 March 2021; accepted 8 April 2021)

ABSTRACT

The seasonal and diurnal variations of cloud systems are profoundly affected by the large-scale and local environments. In this study, a one-year-long simulation was conducted using a two-dimensional cloud-resolving model over the Eastern Tibetan Plateau (ETP) and two subregions of Eastern China: Southern East China and Central East China. Deep convective clouds (DCCs) rarely occur in the cold season over ETP, whereas DCCs appear in Eastern China throughout the year, and the ETP DCCs are approximately 20%–30% shallower than those over Eastern China. Most strong rainfall events (precipitation intensity, PI> 2.5 mm $h^{-1}$) in Eastern China are related to warm-season DCCs with ice cloud processes. Because of the high elevation of the ETP, the warm-season freezing level is lower than in Eastern China, providing favorable conditions for ice cloud processes. DCCs are responsible for the diurnal variations of warm-season rainfall in all three regions. Warm-season DCCs over the ETP have the greatest total cloud water content and frequency in the afternoon, resulting in an afternoon rainfall peak. In addition, rainfall events in the ETP also exhibit a nocturnal peak in spring, summer, and autumn due to DCCs. Strong surface heat fluxes around noon can trigger or promote DCCs in spring, summer, and autumn over the ETP but produce only cumulus clouds in winter due to the cold and dry environment.

**Key words:** the Tibetan Plateau, convective system, seasonal variation, diurnal variation

**Citation:** Chen, J. H., X. Q. Wu, C. S. Lu, and Y. Yin, 2022: Seasonal and diurnal variations of cloud systems over the eastern Tibetan Plateau and East China: A cloud-resolving model study. *Adv. Atmos. Sci.*, **39**(7), 1034–1049, https://doi.org/10.1007/s00376-021-0391-9.

**Article Highlights:**

- The Tibetan Plateau (TP) experiences more significant seasonal and diurnal variations of cloud and precipitation than East China.
- Deep convection in the TP causes the rainfall noon and nighttime peaks in the warm season, while it rarely occurs in the cold season.
- Surface heat fluxes at noon in the eastern TP can promote deep convective clouds in the warm season and result in cumulus in winter.

## 1. Introduction

Due to its lofty and expansive topography, the Tibetan Plateau (TP) is an important boreal summer heat source and winter heat sink (Luo and Yanai, 1984; Zhao and Chen, 2001; Wu et al., 2012; Ge et al., 2019, Wang et al., 2019). During the warm season, the TP acts as a substantial heating source in the middle troposphere and provides an effective driving force for upward motions, which could constitute a complementary forcing for cloud development and even play a critical role in triggering deep convection over the TP (Luo and Yanai, 1983, 1984; Chen et al., 2017b; Fu et al., 2020; Li et al, 2020a). On the other hand, due to its expansive surface area, the TP becomes a vast heat sink in winter (Yanai and Tomita, 1998; Wu et al., 2019), stabilizing the atmosphere and imposing a detrimental effect on cloud development. These local environmental characteristics related to the TP topography, as well as the large-scale circulation, lead to distinct seasonal variations in the cloud sys-

※ This paper is a contribution to the special issue on Third Pole Atmospheric Physics, Chemistry, and Hydrology.

* Corresponding author: Jinghua CHEN
Email: jhchen@nuist.edu.cn

© Institute of Atmospheric Physics/Chinese Academy of Sciences, and Science Press and Springer-Verlag GmbH Germany, part of Springer Nature 2022

tem over this region.

Previous studies have suggested that precipitation over the TP, especially heavy rainfall, shows a strong relationship with moisture transported from the south (e.g., Zhang et al., 2017). This process is closely related to the circulation and moisture conditions over the Indian subcontinent, and these conditions depend on the activity of the Indian summer monsoon (ISM). Similarly, under the influence of the East Asia Monsoon (EAM), the cloud features (e.g., cloud cover, cloud water, precipitation) over East China (EC) show seasonal variations (Huang and Chan, 2012). During the warm season, water vapor is transported from the ocean to EC by the EAM circulation, increasing the cloud water content and bringing plenty of precipitation. Therefore, drastic seasonal variations in the cloud system over EC are expected (Ding, 1992; Chen et al., 2011).

Clouds serve an important regulatory function in the Earth-atmosphere energy balance by absorbing or reflecting the radiation. Clouds also play a key role in the water cycle and modify the energy budget by releasing/absorbing latent heat in water phase transition processes during cloud generation and precipitation (Dai et al., 1999; Dai, 2001). In this context, the macroscopic climatological properties of clouds (e. g., cloud cover, cloud water path) over EC have been widely studied (Dai et al., 2007; Zhou et al., 2008). Precipitation over most of China occurs mainly from June to August (Tao and Chen, 1987; Ding, 1992) and shows diurnal variations during summer (Dai et al., 2007; Chen et al., 2016, 2018a); hence, most previous studies focused on the warm-season precipitation characteristics (Zhou et al., 2008). It has been reported that diurnal variations of the daily precipitation have been obtained over most parts of EC. For example, a late-afternoon maximum over Southeast and Northeast China and a near-midnight maximum over the eastern periphery of the Tibetan Plateau are seen in rain gauge measurements (Zhou et al., 2008). Nocturnal precipitation has also been reported in previous studies (e.g., Singh and Nakamura, 2009; Chen et al., 2018b). Clouds and precipitation are closely linked to the large-scale circulation and local environment (e.g., land use, terrain), and thus, their characteristics vary regionally (Dai, 2001; Dai et al., 2007; Chen et al., 2017a). In particular, the topography of the TP (e.g, through surface heating and terrain blocking) profoundly affects the seasonal variations and diurnal structures of cloud systems and precipitation (Fujinami et al., 2005; Xu and Zipser, 2011). However, the detailed and systematic seasonal characteristics of the cloud systems over the TP, e.g., the cloud properties that caused the diurnal cycle of precipitation in different seasons, still need to be further investigated.The objectives of this study are to simulate the seasonal and diurnal variations of clouds and precipitation over two distinct regions (the ETP and EC) using a cloud-resolving model (CRM) and to understand the impacts of large-scale circulation, topography, and physical processes on the precipitation and cloud characteristics therein. This paper is organized as follows. Section 2 describes the datasets and model configuration. The simulated and observed seasonal and diurnal variations of precipitation and clouds over the ETP and EC are discussed in sections 3, 4, and 5, respectively. A summary and discussion are given in section 6.

## 2. Datasets and model configuration

### 2.1. *Model description*

Wu and Guimond (2006) compared the results from two- and three-dimensional simulations and suggested that the resulting cloud characteristics and precipitation, and the cloud thermal dynamical properties did not exhibit significant differences. Therefore, as this study focuses mostly on cloud properties and does not investigate cloud momentum processes, a two-dimensional CRM is employed to conduct the year-long cloud-scale simulation in this study. The CRM is an anelastic cloud model originally developed by Clark et al. (1996) with large-scale forcing and the modifications to physical processes for the long-term simulations of cloud systems (e.g., Grabowski et al., 1996; Wu et al., 1998, 1999, 2007). The model incorporates the Kessler-type bulk warm rain parameterization (Kessler, 1969) and the Koenig-Murray bulk ice parameterization (Koenig and Murray, 1976). Also, two classes of ice referred to as ice A and ice B, are considered by the CRM, for which both the mixing ratio and the number concentration equations are solved. The ice A field (typically associated with unrimed or lightly rimed ice particles) is formed by the heterogeneous nucleation of pristine ice crystals, while the ice B field, which is usually associated with heavily rimed, high-density particles (e.g., graupel) with a rapid falling speed, originates from the interaction of the rain field with the ice A field. Periodic boundary conditions are employed in the model. The surface heat fluxes in the model are calculated by the parameterization of Liu et al. (1979), however, this parameterization was originally developed for tropical ocean regions and is not suitable over land. Hence, for simplification, the surface heat fluxes in the CRM are prescribed by the ERA-Interim (hereafter, ERAINT, Dee et al., 2011) surface heat flux dataset. More details about this model can be found in the related literature (e.g., Clark et al., 1996; Chen et al., 2017a).

### 2.2. *Data and experimental design*

The CRM is driven by large-scale advection terms, which mimic the effects of the large-scale flow on the temperature and moisture fields (e.g., Yanai et al., 1973). Here, the large-scale horizontal and vertical advection of temperature and moisture are computed from the ERAINT reanalysis (Dee et al., 2011). Furthermore, according to Yanai and Tomita (1998), the calculation results are sensitive to the vertical velocity, therefore, the vertical velocity is recalculated from the horizontal divergence by vertically integrating the continuity equations. Detailed descriptions of the calculation processes are provided in Yanai and Tomita (1998) and

Chen et al. (2015).

The performance of the numerical models is closely related to the driving dataset and uncertainties of the driving data will be introduced into the simulation results. Due to the extremely high elevation and complex terrain, the satellite datasets, which are an important data source for the reanalysis product, have greater uncertainties over the TP. Compared with the western part of the TP, the ETP features lower elevation and has more ground-based observational stations (Wu and Gao, 2013), which also is an important data source for the reanalysis products and can be helpful to assess the model performance. Therefore, the ETP is selected to investigate the seasonal cloud variations over the TP. Located to the east of TP, the EC has lower elevation and less complex terrain and the weather and climate are profoundly affected by the EAM (Ding, 1992). Southern East China (SEC) and Central East China (CEC) are influenced by the advance of EAM to different degrees. Between these two regions, the SCN is affected by the monsoon circulation first in early May, with the effects of EAM fading in September (Ding and Chan, 2005). In contrast, the CEC is an area of flat topography in EC that is meteorologically famous for the Meiyu period during early summer, which is a distinct seasonal characteristic for this region. The ETP, SEC, and CEC are shown in Fig. 1. Since these three regions experience different circulation patterns and moisture conditions, they exhibit distinct cloud and precipitation conditions. To account for these differences, a one-year simulation (2010) is conducted separately for each region to examine the physical processes responsible for these cloud variations. All the simulations of these three regions have a spatial resolution of 3 km and a timestep of 1 second and the result was stored every 15 minutes.

## 3. Seasonal variations of precipitation and clouds

Figure 2 shows the year-long daily precipitation from simulations, Tropical Rainfall Measuring Mission (TRMM) observations, and the ERAINT reanalysis. The CRM successfully captured the seasonal precipitation variations in the SEC, CEC, and ETP and shows the best performance in the CEC, which displays the highest correlation coefficient (0.44, with the TRMM dataset) among all the regions. Compared to the TRMM dataset, the CRM underestimates the heavy rainfall events over these three regions (e.g., 21/May in the SEC, 17/Dec in the CEC, and 21/May in the ETP, Fig. 2). The large-scale forcing used to drive the model is computed from the ERAINT reanalysis dataset. Therefore, the evolution of the simulated precipitation is similar to that of the ERAINT (Fig. 2), indicating that the uncertainties in the reanalysis dataset can be brought into the model results. For example, when the reanalysis becomes unreliable (e.g., the rainfall event around 8 October in the SEC), the model does not produce reasonable precipitation. Moreover, the ETP experiences a dryer climate than the CEC and SEC (Fig. 2), and the precipitation is mostly concentrated in the period from May to August. Heavy rainfall events (>10 mm $d^{-1}$) could occur during the cold season (e.g., December) in the flat regions (e.g., SEC and CEC). Compared with the CEC and SEC, the model and the ERAINT reanalysis show wet biases over the ETP (Fig. 2c). According to Gao and Liu (2013), TRMM precipitation generally tends to underestimate heavy rainfall (>10 mm $d^{-1}$) and overestimate other rainfall events. These features would introduce some uncertainties into the assessment of the model performance of rainfall. Overall, the CRM captures the evolutionary features of the seasonal rainfall over these three regions with some biases in the rainfall amount (Fig. 2).

Figure 3 presents monthly averaged profiles of the total cloud water content (TCWC) and the temperature for the three regions. The evolutionary characteristics of the temperature and clouds for the CEC and SEC show the typical seasonality of a summer monsoon climate. The temperatures of the two flat regions reach their maximum values in summer (June, July, and August, or JJA), and the highest monthly

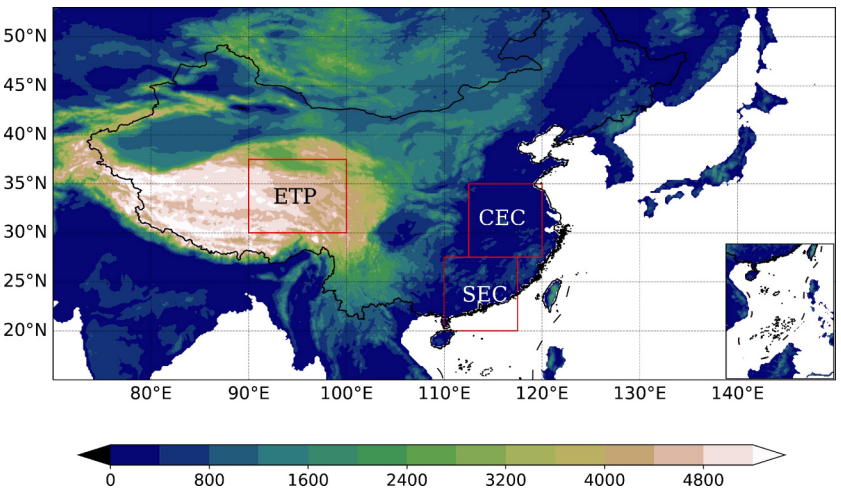


**Fig. 1.** Topography (m) of the domain and the selected regions: SEC, CEC, and ETP, marked with boxes.

near-surface temperature can exceed 25°C (Figs. 3b and d). Besides, the level of the maximum TCWC in the SEC increases beginning in April (Fig. 3a) and lasting through early summer. In contrast, due to its relatively high elevation, the ETP near-surface temperature is much lower than that of the lowland regions (e.g., SEC and CEC). When the warm season arrives, clouds become active in the ETP (Fig. 3e), but the clouds over the ETP do not develop nearly as high as those over the flat regions (Figs. 3a, 3c, and 3e). Furthermore, the monthly domain-averaged near-surface temperature in the ETP can drop below 10°C even in the warmest month (July, Fig. 3f), and the temperature drops to 0°C at just hundreds of meters above ground level (AGL). This feature implies that the ice cloud processes can occur at a lower level in the ETP. A simulation study (Chen et al., 2017a) suggested that the cold cloud microphysical process can occur below 1 km AGL during the warm season in the ETP, which is much lower than that over the lowlands (over 4 km AGL).

The rainfall in the CEC is profoundly affected by the EAM and reaches its maximum value in summer (Ding and Chan, 2005). However, the cold-season TCWC in the CEC is not much smaller than the warm-season TCWC (Fig. 3c). This is possibly related to the quasi-stationary front, which can promote the cloud and precipitation and even lead to persistent extreme precipitation events (Chen and Zhai, 2015). The monthly averaged cloud liquid water content (LWC) and ice water content (IWC) are examined in Fig. 4. The level of the maximum LWC increases in May, when a thin cloud layer appears a few hundred meters above the surface over the CEC (Fig. 4c). By contrast, the maximum monthly averaged IWC in the CEC appears in late winter (February, Fig. 4d). The altitude of the maximum IWC in the CEC increases as the weather warms (Fig. 4d). Besides, the maximum LWC level in the SEC can extend as high as 4 km AGL in winter (Fig. 4a), which corresponds to the freezing level (Fig. 3b). In contrast, the maximum IWC altitude in SEC increases in the warm season and can be as high as 10 km AGL in June, which suggests that deep cloud systems can develop higher in the warm season than in the cold season (Chen et al., 2017a). Over the ETP, the level of the maximum LWC is below 1 km AGL (Fig. 4e) because of the low temperature therein (Fig. 3f), with the maximum IWC occurring at approximately 4 km AGL in June (Fig. 4f), which is much lower than the maximum IWC level over the flat regions (8 km AGL in CEC and 10 km AGL in SEC, Figs. 4b and 4d). Additionally, two layers of LWC are obtained over the ETP and the lower layer has a greater LWC than the upper layer. Previous studies found that shallow cumulus clouds are an important cloud type and are frequent in the warm season over the TP (Li et al., 2004; Li and Zhang, 2016). This suggests that the lower LWC layer over the ETP is largely caused by shallow cumulus clouds.

The frequencies of the cloud top and base altitudes for all cloud grids among the different regions are presented in Fig. 5. Here, the frequency of each cloud cell is defined as the ratio of cloud cell grids to the total grids of this region in the domain. A deep cloud system is usually characterized as having a low cloud base and a high cloud top. When deep clouds are frequent, a left-leaning plume shape will appear in Fig. 5. This feature is detected in spring, summer, and autumn in the CEC (Figs. 5e-g) and in spring and summer in the ETP (Figs. 5i and 5j) though at a considerably lower height (e.g., 7 vs. 12 km), suggesting that deep clouds (e.g., deep convective clouds) prevail during these seasons in these regions. Figure 5h also shows that there are frequent deep clouds as well as other types of clouds, which disturbs the left-leaning distribution of the cloud frequency. Chen et al. (2016, 2018a) suggested that the deep cloud systems are active in the warm season in southern China. However, a left-leaning plume structure is not found in Figs. 5a–d in the SEC, which is possibly caused by the fact that the SEC includes parts of the ocean. The top of the deep cloud system is over 10 km AGL in the CEC and below 8 km AGL in the ETP. The deepest cloud depth (mostly deep convective clouds) exceeds 10 km in the CEC and has no dramatic seasonal differences among spring, summer, and autumn (Figs. 5e–g). The deep cloud depth over the ETP is approximately 20%–30% shallower than that over the CEC and has an increasing tendency of approximately 10% from spring to summer. This finding suggests that clouds can develop higher and become more vigorous in the warm season because of the favorable moisture conditions related to the large-scale circulation and the enhanced surface heat fluxes, which agrees with the results of the modeling sensitivity study and observations (Chen et al., 2019, 2020). A left-leaning plume structure is detected below 6 km AGL in Fig. 5k, which is not a typical cloud top height or depth for deep convection. When winter arrives, the development of clouds over the ETP is substantially restricted (Fig. 5l), which is primarily due to the reduced surface heating and moisture coincident due to the retreat of the ISM.

Benefiting from the humid and warm environment, clouds in the SEC are more active and can develop to a higher level throughout the year than the clouds in the other two regions. For example, clouds with a depth of greater than 8 km can develop to 16 km AGL over the SEC during summer (Fig. 5b). Besides, there are seasonal variations in the deep cloud top over the SEC, with the maximum appearing in summer and the minimum in winter (Figs. 5a–d). The deep cloud shows the highest cloud top in summer and the lowest cloud top in winter in SEC (Figs. 5a–d). The deep cloud top in the CEC does not show significant seasonal variations and is about 4 km lower than that in the SEC. Typical deep convection, characterized by a cloud base below 1 km AGL and a cloud top exceeding10 km AGL, can occur throughout the year in the CEC (Figs. 5e–h) and it is responsible for a lower percentage of the total clouds in summer (Fig. 5f). Moreover, other types of deep clouds, having a cloud base at approximately 2 km AGL and a depth of 6–8 km, can develop in the CEC during spring, autumn, and winter. These clouds with great cloud depths have consider-

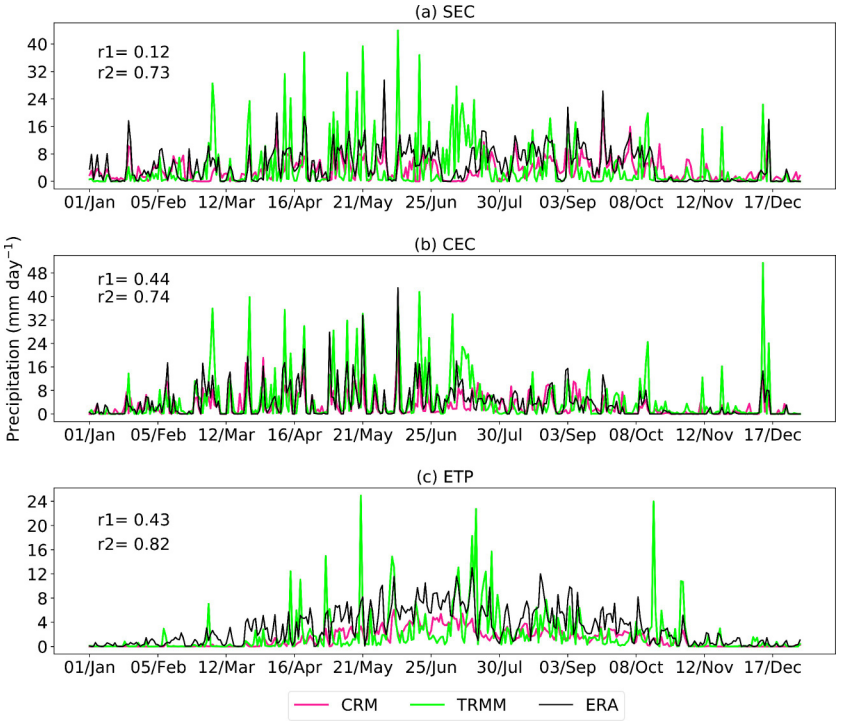


**Fig. 2.** Daily precipitation (mm d$^{-1}$) from the TRMM (green) dataset, ERAINT (black) and simulations (pink) for the SEC (a), CEC (b) and ETP (c). Letters r1 and r2 in the legend are the correlation coefficients between the CRM and the TRMM, and the ERAINT respectively.

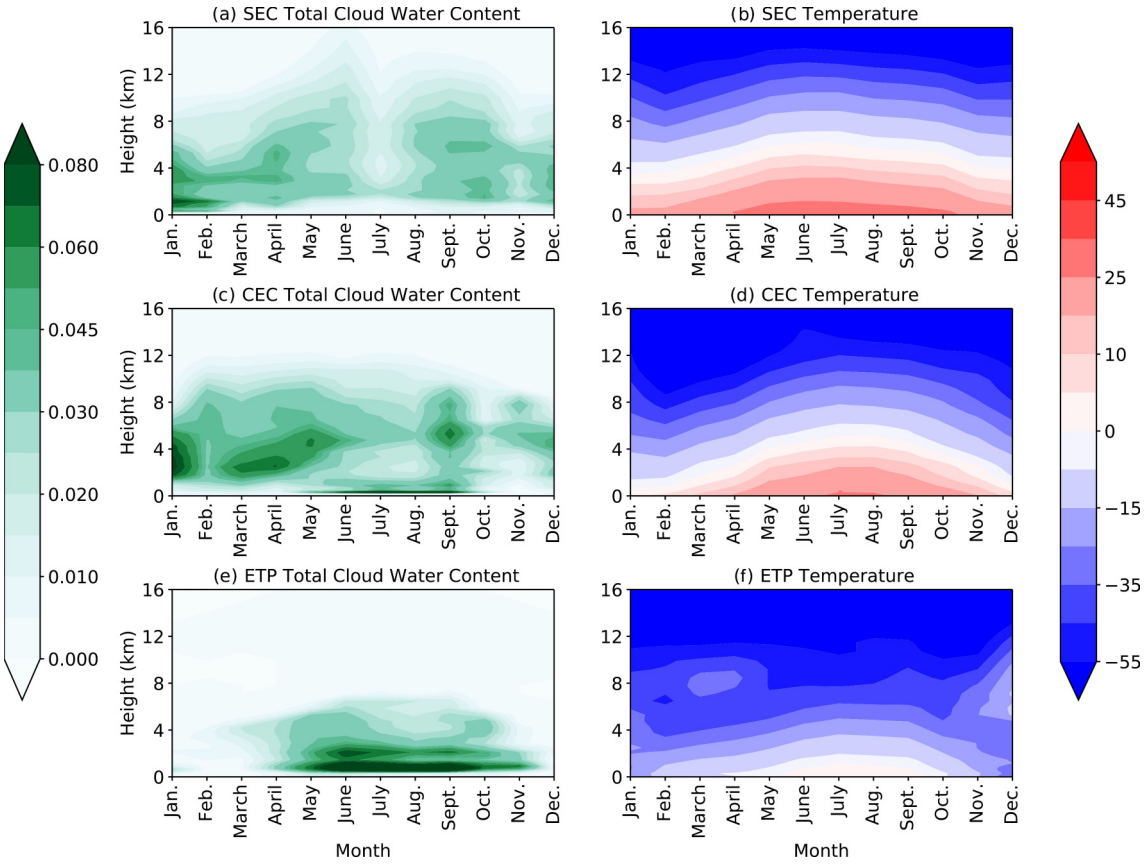


**Fig. 3.** Monthly averaged total cloud water content (g kg$^{-1}$) and temperature (°C) for the SEC (a, b), CEC (c, d), and ETP (e, f).

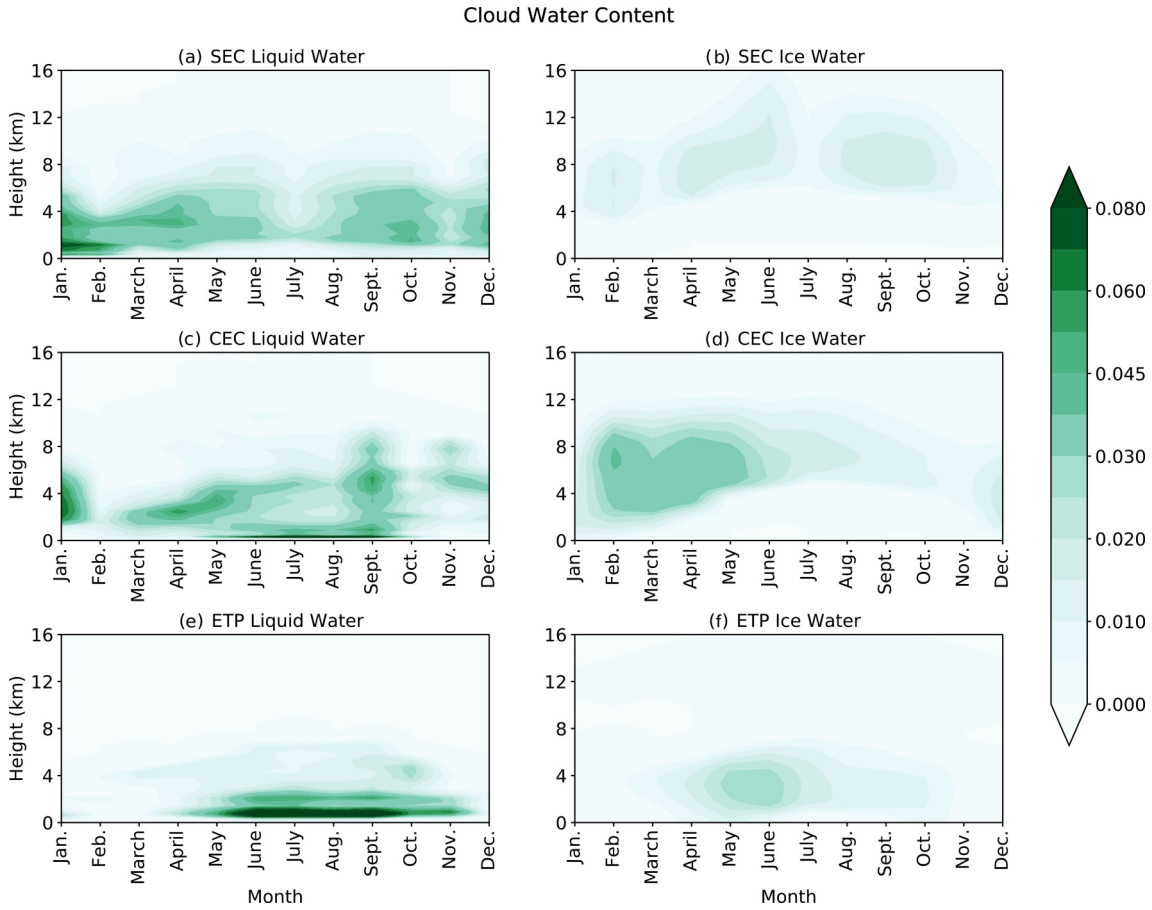


**Fig. 4.** Monthly averaged liquid water content and ice water content (g kg$^{-1}$) for the SEC (a, b), CEC (c, d), and ETP (e, f).

able precipitation capacities and are mostly deep stratiform clouds generated during synoptic processes (e.g., frontal systems). For the ETP, the deep cloud (cloud depth >5 km) top shrinks dramatically to below 8 km AGL (Figs. 5i–k). The cloud depth over the ETP shows seasonal variations with the thinnest depth in winter and the deepest depth during summer; this behavior is largely related to the local thermal heating and moisture supply due to the large-scale circulation in this region. Compared with the results for the lowland regions (e.g., CEC and SEC), the deepest cloud depth over the ETP is shallower, being only 60%–70% of that over the lowland during the same season (e.g., Fig. 5). These results are consistent with satellite observations (Qie et al., 2014). Deep cloud systems rarely develop in the ETP during winter because of the dry, cold environment, and the development of all cloud types is restricted (Fig. 5l). It is worth noting that a maximum frequency appears at the lower-left corner of Figs. 5i–l, which largely reflects the high frequency of cumulus clouds with small cloud depths in the ETP throughout the year.

## 4. Diurnal variations of precipitation and clouds

The diurnal variations of precipitation and clouds are important factors for the local weather and climate (Zhou et al., 2008). The CRM output provides an opportunity to examine the diurnal variations of precipitation and cloud concurrently. The precipitation intensity (PI) is an important characteristic of the cloud system. For example, deep cloud systems primarily produce the greatest PI. Here, rainfall events in each region are classified into five types based on the domain-averaged precipitation intensity of the three regions (Table 1). These five types (I-V) are successively defined as little, small, middle, strong, and heavy rain events. Based on this classification, the frequencies of all five types of rainfall events for all three regions were obtained using the 15-minute interval model output, as shown in Fig. 6. Heavy rainfall (type V) events in the SEC can account for almost 15% of all precipitation in summer but account for less than 3% of the total in winter, which corresponds to the seasonal variation of deep clouds (Fig. 5). The frequencies of rainfall events with a PI below 2.5 mm h$^{-1}$ do not show dramatic seasonal variations in the SEC (Figs. 6a–d), indicating that these clouds, except deep clouds, occur at similar frequencies in different seasons. By contrast, in the CEC, each rainfall type shows seasonal frequency variations. The frequency of heavy rainfall (type V) events reaches its maximum in the warm season in the CEC, where the frequency of heavy rainfall is approximately 10% in summer, which is

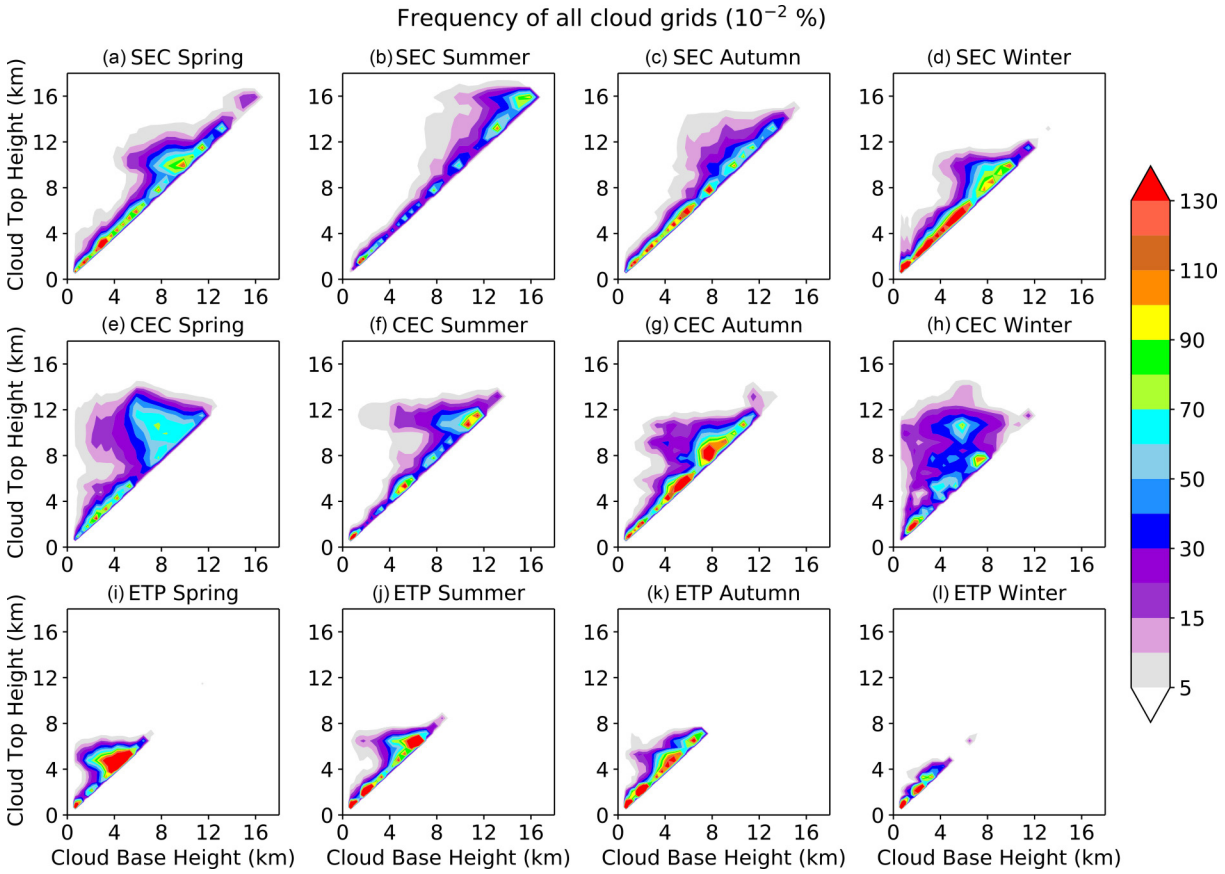


**Fig. 5.** Seasonal frequency of cloud base and cloud height all cloud grids for the SEC, CEC, and ETP of the year 2010.

**Table 1**. Classification of the rainfall events based on the domain-averaged precipitation intensity (PI).

| Type | I | II | III | IV | V |
|---|---|---|---|---|---|
| PI (mm $h^{-1}$) | PI ⩽ 0.2 | 0.2 < PI ⩽ 1 | 1 < PI ⩽ 2.5 | 2.5 < PI ⩽ 5 | PI > 5 |

lower than that in the SEC (Figs. 6b and 6f). Dramatic seasonal variations are detected for all the rainfall types in the ETP (Figs. 6i–k). Type V rainfall, which is produced primarily by deep convective clouds in the ETP, is most frequent in summer, followed by spring and autumn, whereas the strongest rainfall type (type V) events rarely occur in winter, suggesting that clouds with a great precipitation capacity seldom occur during this season. These results agree with the frequency of deep clouds shown in Figs. 5i–l.

The frequency of heavy rainfall shows a diurnal variations pattern with a noon peak in spring and a late afternoon peak in summer over the SEC (Figs. 6a–b). These results suggest that rainfall events with the greatest PI (type V) tend to occur around noon (late afternoon) in spring (summer) in the SEC, which agrees with the observational results (Zhou et al., 2008). Chen et al. (2016, 2018a) also found that the SEC rainfall usually shows an afternoon peak of rainfall in summer, which strongly indicates that deep convection is highly active. However, the other types of precipitation do not show significant diurnal variation patterns in spring, autumn, or winter in the SEC (Fig. 6d). Compared with spring and winter, summer and autumn are characterized by a pronounced diurnal precipitation cycle in the CEC (Figs. 6e–h). The frequency of little rainfall (type I) in the warm season shows a diurnal cycle structure with a peak at night in the CEC (Fig. 6f). The diurnal cycle of warm-season precipitation is also seen by the ground-based observational datasets in the Middle Yangtze River Valley (Yu et al., 2007; Zhou et al., 2008). In contrast, the other types of rainfall events in the CEC during the warm season show frequency of occurrence peaks around noon. The greater the PI, the more obvious the solitary peak structure (Fig. 6f). The precipitation, which is estimated by Artificial Neural Networks and Tropical Rainfall Measuring Mission 3B42 (TRMM) (Zhou et al., 2008), failed to capture the early morning peak in the diurnal precipitation frequency cycle in the Middle Yangtze River valley (Zhou et al., 2008). The early morning precipitation frequency peak determined in this study is composed mostly of the little rainfall events (type I, Fig. 6f), which implies that the TRMM dataset may underestimate the frequency of little rain events in the CEC. In contrast, the diurnal cycle signals of type II-V rainfall events

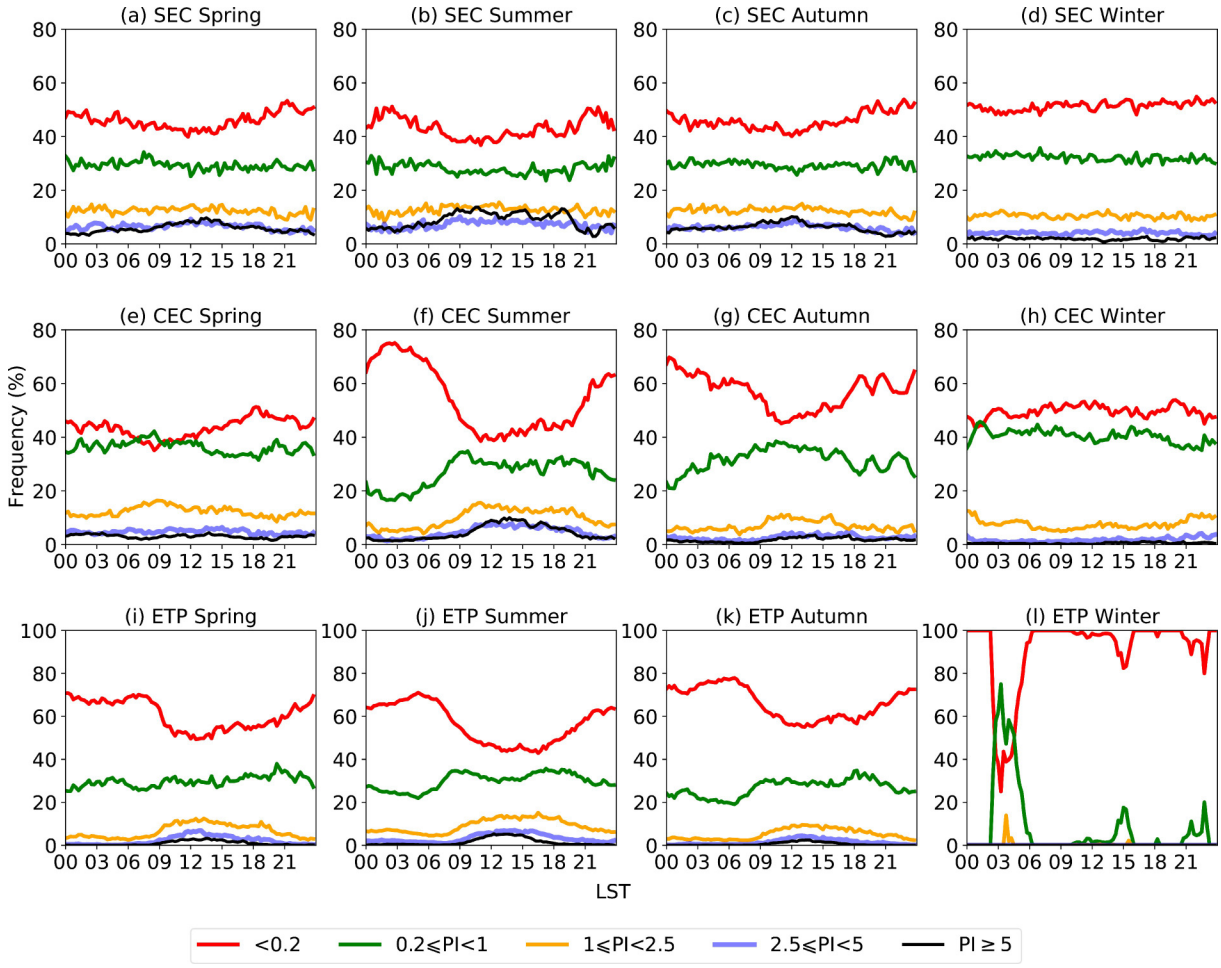


**Fig. 6.** Diurnal cycle of the frequency of different precipitation intensities (mm $h^{-1}$) in four seasons for the SEC (a–d), the CEC (e–h), and the ETP (i–l).

weaken in autumn and disappear in winter in the CEC (Figs. 6g–h). Similarly, the frequencies of strong and heavy rainfall events (type IV and V) in the CEC decrease in autumn and winter. However, the CEC small rainfall events (type II) frequency reaches its maximum values in winter with no dramatic diurnal variations. Under the influence of the East Asia summer monsoon, both the CEC and SEC experience the most rainfall in summer; rainfall events with PI greater than 2.5 mm $h^{-1}$ reach a noon peak in the CEC and an afternoon peak in the SEC. According to Xu and Zipser (2011), deep convective clouds have peaks around noon in the CEC and the late afternoon in the SEC, which implies that deep convective clouds make important contributions to the frequency peak of warm-season strong and heavy rainfall events at approximately noon (afternoon) in the CEC (SEC).

Compared to those in the lowland regions, the frequencies of all rainfall types in the ETP (except small rainfall (type II) events, which do not display a pronounced diurnal frequency in spring, summer, and autumn) show diurnal variations in spring, summer, and autumn (Figs. 6i–k). In this region, types III-V rainfall events are collectively considered great rainfall events. Great rainfall events rarely occur in winter in the ETP (Fig. 6l), leading to a nearly rainless winter, as noted in the TRMM dataset (Fig. 2c). Great rainfall events in the ETP being to appear in spring with a frequency peak around noon (Fig. 6i). When summer arrives, great rainfall events become more frequent (Fig. 6j) and show a diurnal frequency variation with a bimodal structure. The main peak is in the afternoon, accounting for over 20% of all rainfall events; there is also a weak secondary peak in the early morning, accounting for less than 10% of the total. Using the TRMM datasets, Fu et al. (2006) found that a strong diurnal cycle of precipitation occurring over the central TP with a peak in the late afternoon and a minimum at approximately 0500 LST (local standard time), confirming the diurnal cycle structure depicted in Fig. 6j and indirectly indicating that most rainfall events on the plateau are convective in summer (Fu et al., 2006).

Deep convection signifies a type of cloud with great precipitation capacity. Here, deep convective clouds are distinguished by the following two criteria: (1) the cloud depth is greater than 10 km over lowland regions (5.5 km over the ETP), and (2) the cloud top is greater than 12 km AGL over lowland regions (6 km AGL over the ETP). This definition considers differences in the cloud depth between the ETP

and the lowland regions (e.g., Fig. 6i). The basic idea behind this definition is that deep convection normally extends vertically through most of the troposphere, and the atmospheric column is much thinner over the ETP than over the lowlands. Compared to adopting a uniform definition for all the regions, our definition can provide more deep convection samples in the ETP. This other method just considers the cloud depth and cloud top, which may regard the thick stratiform cloud as DCC and cause some uncertainties.

Figures 7 and 8 show the diurnal cycles of the averaged profiles of the frequency and TCWC profiles of the DCCs, respectively, for each season over the SEC, CEC, and ETP. The TCWC can be used to measure the intensity of deep convection and rainfall (Chakraborty et al., 2016), which helps understand the diurnal precipitation variations, as shown in Fig. 6. The averaged profiles of the TCWC and frequency of deep convective clouds show seasonal variations corresponding to great rainfall events (Figs. 6, 7 and 8). Both the SEC and CEC feature DCCs have a high TCWC and high frequency in summer (Figs. 7b, 7f and 8b, 8f), which agrees with the seasonal variations of great rainfall events (type III-V, Figs. 6b and 6f). It is worth noting that DCCs over the CEC show a winter frequency peak. However, the TCWC of the CEC winter deep convection is smaller than those in summer. Considering that DCCs are filtered by cloud depth and cloud top, the CEC winter DCCs may include some thick stratiform clouds. In contrast, the DCCs over the SEC show a maximum frequency and TCWC around noon in summer (Figs. 7b and 8b), while great rainfall (type III-V) events show a high frequency in the afternoon (Fig. 6b). The different peak time of the DCC's frequency and TCWC and rainfall implies that other deep cloud systems may contribute to the afternoon rainfall peak. Unfortunately, the DCC definition may raise some uncertainties regarding the DCC peak time. The TCWC of the summer deep convection reaches its maximum around noon at approximately 8 km AGL in the CEC, whereas the maximum TCWC can extend to 10 km AGL between noon and late afternoon in the SEC (Figs. 8b and 8f). However, a previous study reported that midsummer rainfall in the CEC peaks in the later afternoon (approximately 1600 LST) (Chen et al., 2009). Figure 7f indicates high-frequency DCCs in the late afternoon, suggesting that the late afternoon peak of rainfall in the CEC (Chen et al., 2009) is related to these high-frequency DCCs. Furthermore, the DCCs over the SEC show a higher maximum TCWC level than those over the CEC in all seasons (Figs. 8a-h), suggesting that the DCCs in the SEC are more energetic than those in the CEC. The TCWC of convective clouds over the lowland regions (e.g., SEC and CEC) shows a diurnal cycle in spring, summer, and autumn but no significant diurnal cycle in winter (Figs. 8d and 8h). However, the frequencies of DCCs in the lowland regions exhibit diurnal variations in the cold season (Figs. 7d and 7h), which could be a pos-

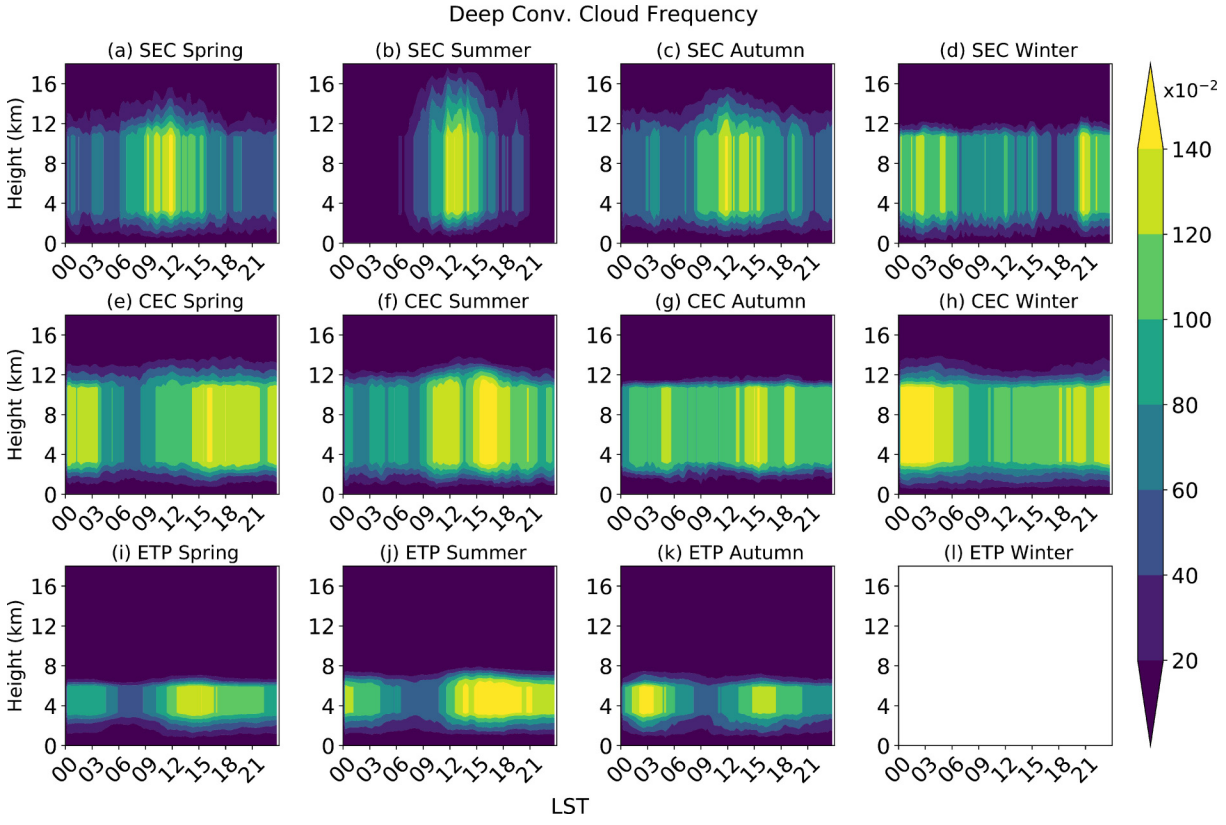


**Fig. 7.** Diurnal cycle of frequency (%) of deep convective clouds in four seasons for the SEC (a–d), the CEC (e–h), and the ETP (i–l). Note that because no deep convective cloud cells could be identified during winter for the ETP, they were removed from the analysis.

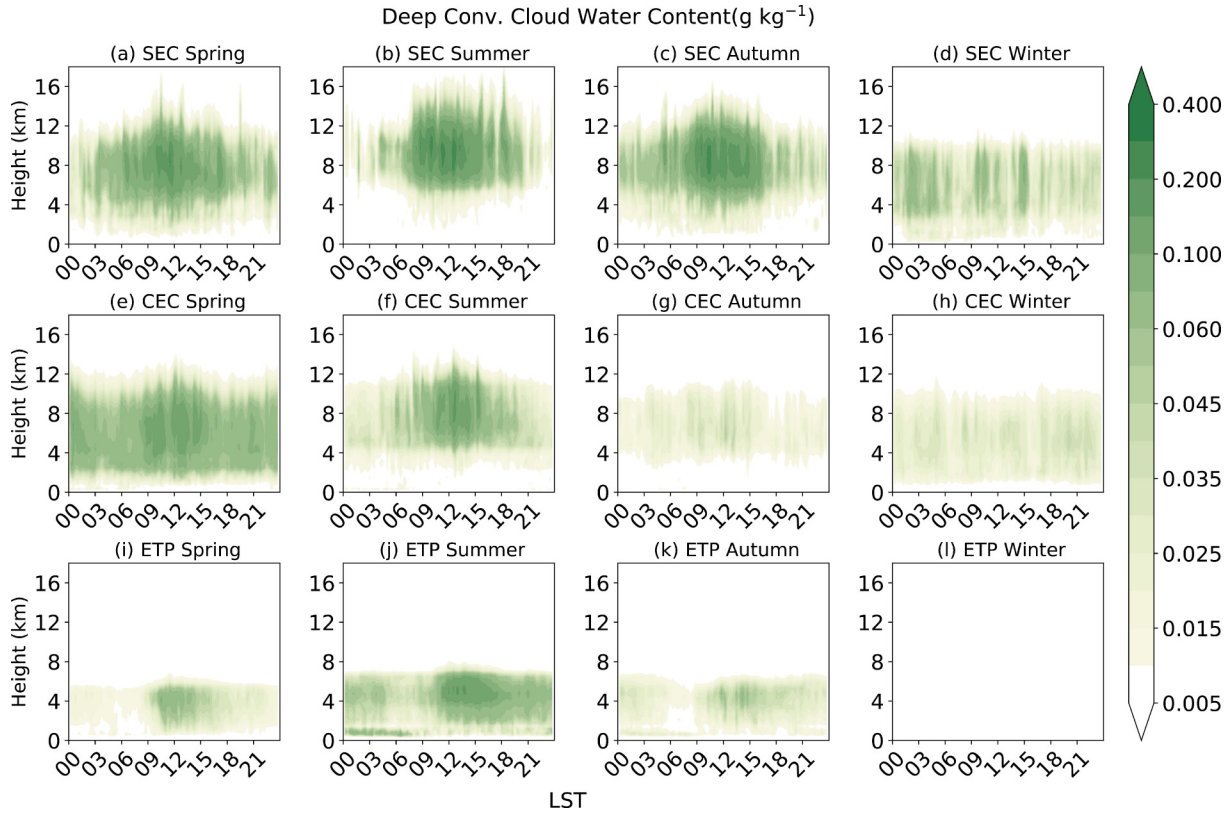


**Fig. 8.** Diurnal cycle of total cloud water content (g kg$^{-1}$) of deep convective clouds in four seasons for the SEC (a–d), the CEC (e–h), and the ETP (i–l). Note that because no deep convective cloud cells could be identified during winter for the ETP, they were removed from the analysis.

sible reason for the cold-season diurnal precipitation cycle, as reported by Huang and Chan (2012).

Figures 5 and 6 show that the ETP features the most significant seasonal cloud frequency and the most dramatic diurnal precipitation cycle among all three regions. These features also appear in the TCWC and frequency of the DCCs (Figs. 7i–l and 8i–l). The most favorable environment for the triggering and development of DCCs over the ETP occur in summer, followed by spring and autumn (Figs. 7i–k and 8i–k). Previous studies reported that deep convection activity and precipitation over the ETP display an afternoon peak because of the influence of the surface heat flux in the warm season (e.g., Chen et al., 2017a, 2018b; Li, 2018). Figure 9 shows diurnal variations with a noon peak in the surface heat fluxes (including sensible heat flux and latent heat flux) in the ETP in each season. Figures 7j and 8j display frequent summer DCCs with a high afternoon TCWC in the ETP, which greatly contribute to the early-afternoon precipitation peak (Fig. 6j). Besides, warm-season nocturnal rainfall in the ETP has been reported by Chen et al. (2018b). Consistent with this finding, the deep convection frequency shows a weak secondary peak at night in the warm season (Fig. 7j). However, nighttime DCCs have a smaller TCWC than afternoon DCCs (Fig. 8j), which implies that nocturnal rainfall events have relatively weak intensity. The warm-season structures (a strong afternoon peak and a hint of a secondary night mode) of the diurnal cycles of the deep convection frequency and TCWC (Figs. 7j and 8j) correspond to the diurnal structure of rainfall events with a PI greater than 2.5 mm h$^{-1}$ (Fig. 6j). According to TRMM observations (Singh and Nakamura, 2009), the precipitation falling over the central TP shows a second peak at midnight in the warm season, which is similar to the diurnal structures of the deep convection TCWC and frequency in the ETP (Figs. 7j and 8j). This similarity suggests that DCCs not only are the primary mechanism responsible for the afternoon precipitation peak but also greatly contribute to the nocturnal precipitation peak. A bimodal structure of the deep convection frequency is detected in spring and autumn (Figs. 7i and 7k) and the maximum frequency in autumn appears during the night (Fig. 7k). However, nocturnal DCCs have small TCWCs (Figs. 8i and 8k), which will reduce their precipitation capacity and possibly lead to weak-intensity rainfall events. Winter does not provide conducive conditions for triggering and development of DCCs in the ETP (Figs. 7l and 8l), largely due to the dry and cold climate therein.

## 5. Diurnal variations of cumulus clouds

In addition to DCCs, shallow clouds (e.g, cumulus clouds, Cu) play an important role in the local Earth-atmosphere energy budget and are one of the dominant cloud types over the TP (Li and Zhang, 2017). Shallow clouds (SC) can transport heat and moisture from near the surface

to the free atmosphere (Wang and Zhang, 2014), thereby ventilating the planetary boundary layer. Moreover, convective clouds over the TP can evolve from shallow, dry convection in the morning to deep, moist convection in the afternoon (Yang et al., 2004). Here, Cu is defined as a cloud column with a depth shallower than 1.5 km and a cloud top height below 6.5 km AGL, excluding thin high clouds (e.g., cirrus). It should be obvious that this method may incorrectly consider stratus or stratocumulus cloud as cumulus. If the non-precipitation cloud of a region is dominated by cumulus, the clouds detected by this method will be mostly cumulus, e.g., as in the ETP. Figure 10 shows the diurnal cycle of the averaged shallow cloud TCWC with different cloud bases. For the SEC, Cu is active throughout the year, and there is no significant pattern in the TCWC diurnal cycle for each season (Figs. 10a–d). The Cu frequency in the SEC shows two maximum layers in spring (Fig. 11a): one is approximately 2 km AGL and another at approximately 3.5 km AGL. In contrast, the other seasons show a singular maximum frequency at approximately 2 km AGL (Figs. 11b–d). Compared to the SEC, Cu in the CEC has a lower TCWC (Figs. 10e–h) and exhibits diurnal variations in both the frequency and the TCWC (Figs. 10e–h and 11e–h). The most frequent season for Cu in the CEC is winter, while Cu has the greatest TCWC in summer (Figs. 11f and 11h). The cloud base of Cu with the maximum TCWC in the CEC increases after 07:00 LST in spring, summer, and autumn (Figs. 10e–g). Moreover, in the CEC, the cloud base of the most frequent Cu in winter is approximately 2 km AGL (Fig. 11h), which is higher than that in the other seasons (Figs. 11e–h). Figures 11e–h show that Cu exhibits antiphase in the diurnal frequency variation with the deep convection frequency (Figs. 7e–h), indicating that the greatest frequency of Cu corresponds to the least frequent deep convection occurrence, and vice versa. Moisture and energy will be transported to the CEC by the monsoon circulation during the warm season (Ding and Chan, 2005), creating a favorable environment for the triggering and development of DCCs. Chen et al. (2013) found that the summer monsoon diurnal cycle can strengthen low-level moisture transport at night by about 20% more than during the day, which can lead to flourishing cloud activity and is responsible for the early morning rainfall peak in the warm-season precipitation. However, DCCs preferentially occur at noon into the afternoon (Li et al., 2020b) (e.g., Figs. 7 and 8). When the monsoon fades in winter, the atmosphere dries, and thus, deep clouds cannot be triggered frequently in the CEC, leading to more opportunities to generate Cu.

The TCWC of Cu in the ETP shows a clear seasonal variation with the maximum in summer, followed by autumn, spring, and winter (Figs. 10i–l). These seasonal variations reflect the moisture and thermal conditions associated with the ISM. The cloud base of Cu with the maximum TCWC increases after 0900 LST and reaches its maximum at

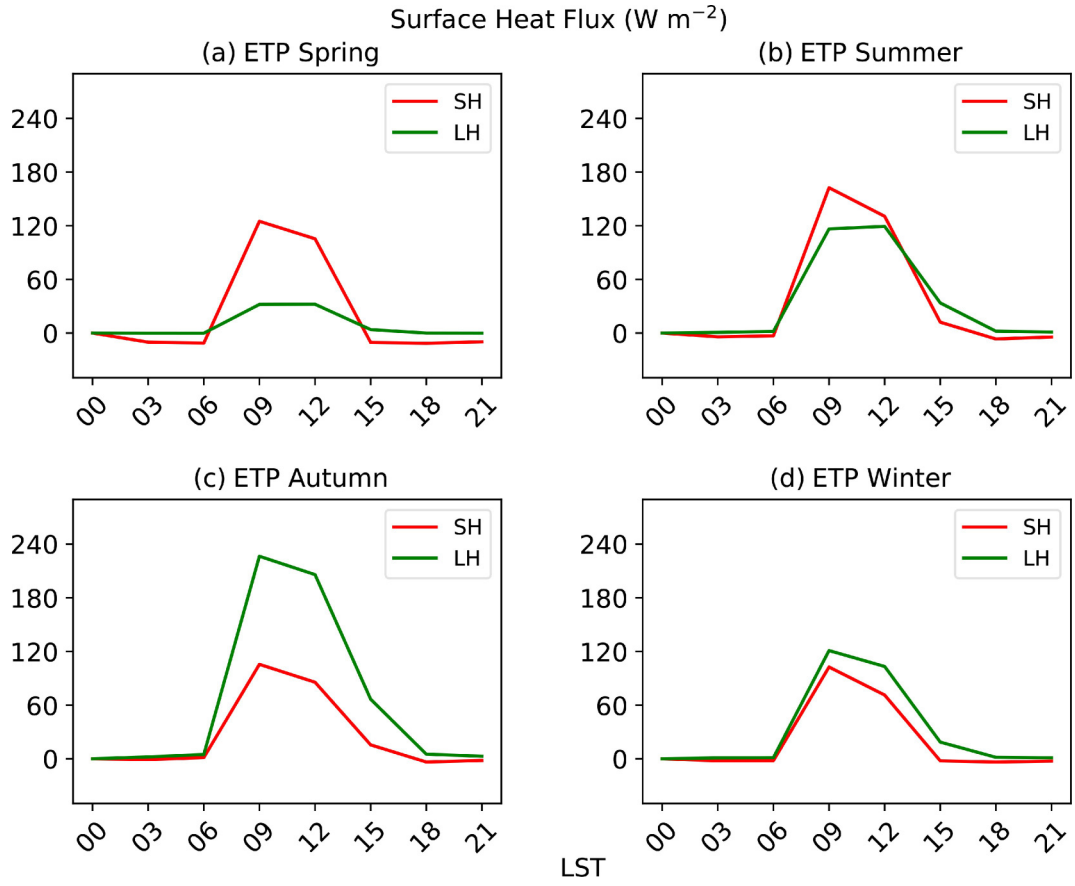


**Fig. 9.** Diurnal cycle of surface sensible heat flux (SH) and latent heat flux (LH) in four seasons over the ETP.

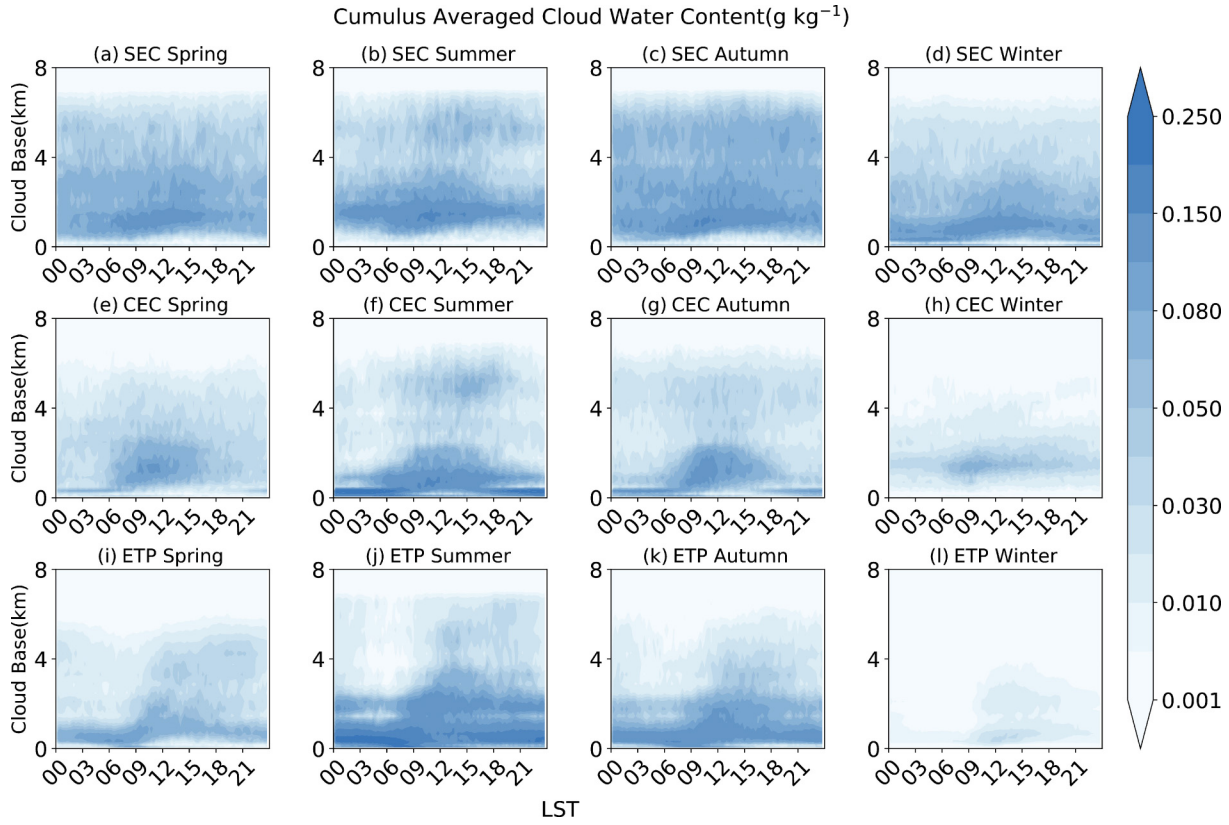


**Fig. 10.** Diurnal cycle of total cloud water content (g kg$^{-1}$) of shallow cumulus in four seasons for the SEC (a–d), the CEC (e–h), and the ETP (i–l).

around noon in the ETP (Figs. 10i–l), which is mostly affected by surface sensible heat flux (Fig. 9). The maximum frequency period of Cu in the ETP is approximately 0700~0800 LST in spring, summer, and autumn, but approximately 1400 LST in winter (Figs. 11i–l). Li and Zhang (2016) suggested that the temperature near the TP surface is warmer than the surrounding atmosphere at the same altitude even during the warm season nights, which results in larger moist static energy and makes for a favorable condition for the Cu development. After sunrise, the solar-heated surface will promote the development of cumulus. However, the cloud will develop deeper than Cu along with the increasing solar radiation. This is a possible reason for the Cu morning peak in the warm season. Moreover, the Cu frequency increases after 1800 LST in spring, summer, and autumn in the ETP. Panels i-k in Figs 6, 7, and 8 show that most DCCs with a high TCWC develop at noon into the afternoon and lead to significant precipitation events. The precipitation process will consume moisture and terminate DCCs. After the convective rainfall, the remnants of DCCs would be a possible contributor to the increase of the Cu's frequency after 1800 LST. The maximum frequency of Cu in the ETP occurs at approximately 1300 LST in winter (Fig. 11l), which corresponds to the period with the strongest surface heat fluxes (Fig. 9l). The maximum frequency and TCWC of DCCs over the ETP in the other seasons are observed around 1300 LST (Figs. 7i–k and 8i–k). According to the results of a sensitivity study by Chen et al. (2019), the surface heat flux plays an important role in the triggering and development of warm-season deep convection and heavy rainfall events. When winter arrives over the ETP, the atmosphere becomes cold and dry, which restricts deep cloud development, especially DCCs. Under these conditions in the ETP, increased surface heating around noon (Fig. 9l) can hardly trigger DCCs in winter, although Cu will develop (Fig. 11l). Moreover, Cu around noon has a much smaller TCWC than the other seasons (Figs. 10i–k), suggesting that Cu can be triggered by surface heating around noon in winter and that their TCWC is small because of the cold and dry environment.

## 6. Conclusion and discussion

The seasonal and diurnal variations of clouds and precipitation over the monsoon areas of East China and the Eastern Tibetan Plateau (ETP) are investigated using a two-dimensional cloud-resolving model. The differences in the seasonal and diurnal variations of clouds between the East China region and the Extended Tibetan Plateau are discussed, and the salient conclusions are summarized as follows.

Affected by the monsoon system, most of the precipitation in the lowlands occurs in the warm season. The deep cloud systems with ice processes over the Southern East

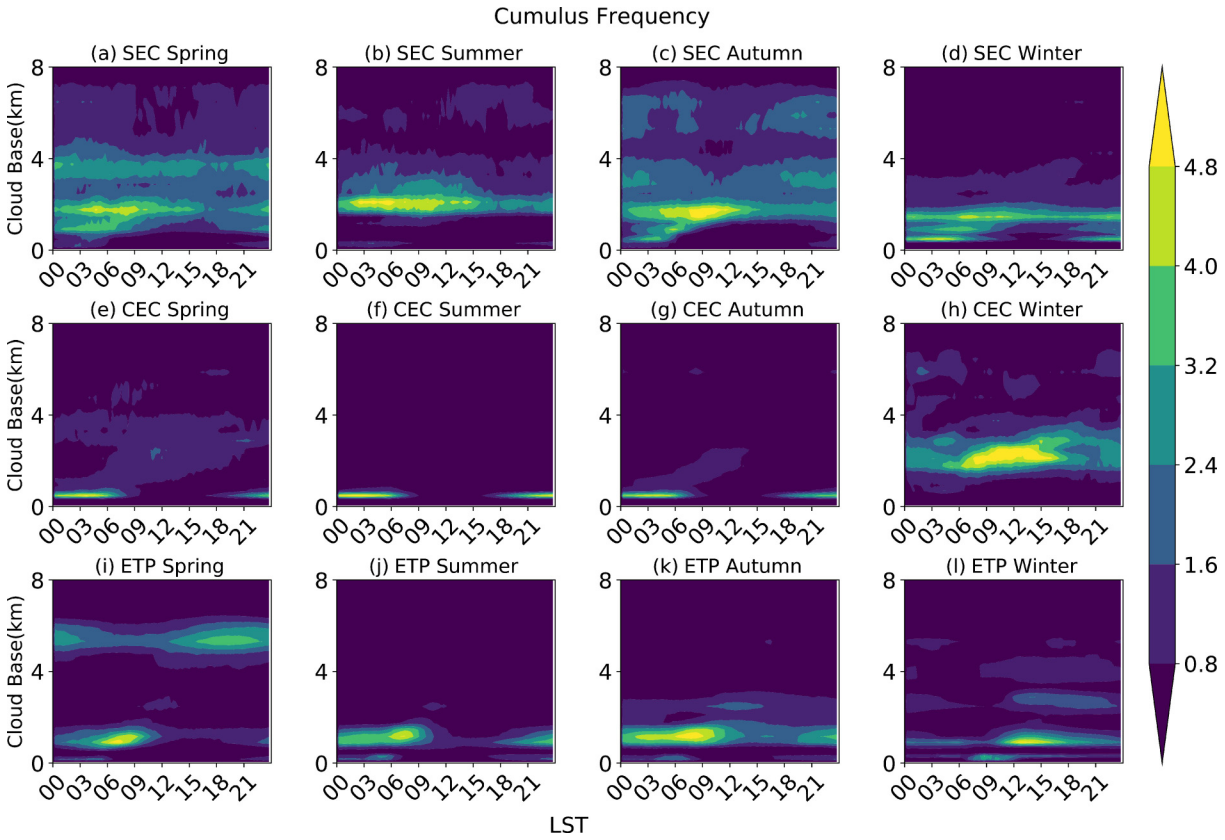


**Fig. 11.** Diurnal cycle of frequency (%) of cumulus in four seasons for the SEC (a–d), the CEC (e–h), and the ETP (i–l).

China (SEC) become active and powerful in May and reach their maximum frequency and intensity in July. Deep convective clouds (DCCs) prevail in spring, summer, and autumn over the Central East China (CEC) and contain the greatest total cloud water content in summer; these convective clouds provide important contributions to warm-season rainfall. Compared to those in the CEC, DCCs in the SEC can extend to a higher level but constitute a smaller percentage of the total cloud cells. However, other deep clouds are frequent in the warm season and can develop to levels above 10 km AGL, potentially contributing to the rainfall in the SEC.

Most of the cloud activity in the ETP occurs from May to October, and most of the precipitation is concentrated in the same period. Ice cloud processes in the ETP can occur in most clouds during the warm season because of the low freezing level due to the low near-surface temperature. Moreover, because of the thin atmospheric column above the elevated terrain characterizing the ETP, most clouds are restricted below 10 km AGL. In this region, DCCs are the most common and have the greatest total cloud water content in summer, which is largely related to the transport of moisture by the large-scale circulation and the strong surface heating effects over the plateau. However, DCCs in the ETP are 20%–30% lower in height than those over the lowland (e.g., the CEC and SEC) because of the terrain effect, and only rarely occur in winter.

Heavy rainfall events (Precipitation Intensity, PI > 5 mm $h^{-1}$) in the SEC show a diurnal cycle with an afternoon peak in spring and summer corresponding to diurnal variations of deep clouds with the greatest precipitation capacity. The frequencies of the great rainfall events (PI > 2.5 mm $h^{-1}$) in the CEC show a diurnal variation pattern with an afternoon peak in the warm season. Moreover, DCCs in the CEC can develop to higher levels in summer and can substantially contribute to summer rainfall. Besides Precipitation Intensity, Yu et al. (2007) found that the rainfall duration is an important factor for the precipitation variations. Considering that the large-scale forcing is calculated based on the ERAINT with a 3-hour interval, the duration of the precipitation event is not examined in this study, which would need to be conducted with a high temporal resolution dataset.

DCCs in the ETP have the greatest total cloud water content and frequency in the afternoon in summer, resulting in a high-frequency peak of the great rainfall events (PI > 2.5 mm $h^{-1}$). In addition to the afternoon peak, great rainfall events (PI > 2.5 mm $h^{-1}$) in the ETP also feature a secondary occurrence maximum at night, which agrees with previous observations (Chen et al., 2018b). Moreover, this nocturnal precipitation peak in the ETP is shared by DCCs, which show second nocturnal peaks in the frequency and total cloud water content.

Shallow cumulus does not show diurnal variations in any season over the SEC. However, the Cu diurnal variations are obtained over the CEC and ETP. Usually, the

cloud base of cumulus with the maximum TCWC increases from 0900 LST to 1300 LST in the CEC and ETP in spring, summer, and autumn. The maximum frequency of cumulus occurs at night during spring, summer, and autumn in the CEC and ETP. In the ETP, cumulus reaches its maximum frequency and total cloud water content around noon in winter, mostly caused by heating due to surface heat fluxes. Strong surface heat fluxes around noon can promote the development of clouds or trigger DCCs under suitable moisture and thermal conditions, particularly in the warm season. However, the surface heat flux around noon can only trigger Cu due to the cold and dry atmosphere of the ETP during the cold season.

The investigation and analysis of cloud systems in this study are based mainly on simulations by a two-dimensional cloud-resolving model. Although the model performance has been investigated over several regions (e.g., the Great Plain of North America, East China, and the Tibetan Plateau) in previous studies (Grabowski et al., 1998; Wu et al., 1998; Chen et al., 2017a, 2019), uncertainties can be caused by the model properties (e.g., periodic boundary conditions, two-dimension assumption) and large-scale forcing. Moreover, the mechanism for the triggering and development of the ETP nocturnal DCCs needs to be further investigated by well-designed three-dimensional numerical experiments.

***Acknowledgements***. This study was supported under the National Key R&D Program of China (Grant No. 2017YFA0604001) and National Science Foundation of China (Grant Nos. 42075067, 41875071, and 41705118), the Second Tibetan Plateau Scientific Expedition and Research (STEP) program (Grant No. 2019QZKK0105), Key research and Development Program of Anhui Province (Grant No. 202004b11020012), China Scholarship Council, the Natural Science Foundation of Jiangsu Province (Grant No. BK20170945), the Open Fund of Key Laboratory of Meteorology and Ecological Environment of Hebei Province and the National Center of Meteorology, Abu Dhabi, UAE under the UAE Research Program for Rain Enhancement Science.

## REFERENCES

Chakraborty, S., A. Adhikari, and A. Maitra, 2016: Rainfall estimation from liquid water content and precipitable water content data over land, ocean and plateau. *Atmospheric Research*, **167**, 265–274, https://doi.org/10.1016/j.atmosres.2015.08.012.

Chen, G. X., W. M. Sha, and T. Iwasaki, 2009: Diurnal variation of precipitation over southeastern China: Spatial distribution and its seasonality. *J. Geophys. Res.*, **114**, D13103, https://doi.org/10.1029/2008JD011103.

Chen, G., Sha, W., Sawada, M., and Iwasaki, T, 2013: Influence of summer monsoon diurnal cycle on moisture transport and precipitation over eastern China. *J. Geophys. Res. Atmos.*, **118**, 3163–3177, https://doi.org/10.1002/jgrd.50337.

Chen, G. X., R. Y. Lan, W. X. Zeng, H. Pan, and W. B. Li, 2018a: Diurnal variations of rainfall in surface and satellite observations at the monsoon coast (South China). *J. Climate*, **31**, 1703–1724, https://doi.org/10.1175/JCLI-D-17-0373.1.

Chen, H. M., R. C. Yu, and Y. Shen, 2016: A new method to compare hourly rainfall between station observations and satellite products over central-eastern China. *Journal of Meteorological Research*, **30**, 737–757, https://doi.org/10.1007/s13351-016-6002-5.

Chen, H. M., J. Li, and R. C. Yu, 2018b: Warm season nocturnal rainfall over the eastern periphery of the Tibetan Plateau and its relationship with rainfall events in adjacent regions. *International Journal of Climatology*, **38**, 4786–4801, https://doi.org/10.1002/joc.5696.

Chen, J. H., X. Q. Wu, Y. Yin, and H. Xiao, 2015: Characteristics of heat sources and clouds over eastern china and the tibetan plateau in boreal summer. *J. Climate*, **28**, 7279–7296, https://doi.org/10.1175/JCLI-D-14-00859.1.

Chen, J. H., X. Q. Wu, Y. Yin, Q. Huang, and H. Xiao, 2017a: Characteristics of cloud systems over the Tibetan Plateau and East China during boreal summer. *J. Climate*, **30**, 3117–3137, https://doi.org/10.1175/JCLI-D-16-0169.1.

Chen, J. H., X. Q. Wu, Y. Yin, C. S. Lu, H. Xiao, Q. Huang, and L. P. Deng, 2019: Thermal effects of the surface heat flux on cloud systems over the Tibetan Plateau in boreal summer. *J. Climate*, **32**, 4699–4714, https://doi.org/10.1175/JCLI-D-18-0604.1.

Chen, J., X. Wu, Y. Yin, and C. Lu, 2020: Large-Scale Circulation Environment and Microphysical Characteristics of the Cloud Systems Over the Tibetan Plateau in Boreal Summer. *Earth and Space Science*, **7**, e2020EA001154, https://doi.org/10.1029/2020EA001154.

Chen, T. C., W. R. Huang, and M. C. Yen, 2011: Interannual variation of the late spring-early summer monsoon rainfall in the Northern Part of the South China Sea. *J. Climate*, **24**, 4295–4313, https://doi.org/10.1175/2011JCLI3930.1.

Chen, Y., and P. M. Zhai, 2015: Synoptic-scale precursors of the East Asia/Pacific teleconnection pattern responsible for persistent extreme precipitation in the Yangtze River Valley. *Quart. J. Roy. Meteor. Soc.*, **141**, 1389–1403, https://doi.org/10.1002/qj.2448.

Chen, Y. L., Y. F. Fu, T. Xian, and X. Pan, 2017b: Characteristics of cloud cluster over the steep southern slopes of the Himalayas observed by CloudSat. *International Journal of Climatology*, **37**, 4043–4052, https://doi.org/10.1002/joc.4992.

Clark, T. L., W. D. Hall, and J. L. Coen, 1996: Source code documentation for the clark-hall cloud-scale model: Code version G3CH01. NCAR Tech. Note NCAR/TN-426+STR, 137 pp.

Dai, A. G., 2001: Global precipitation and thunderstorm frequencies. Part II: Diurnal variations. *J. Climate*, **14**, 1112–1128, https://doi.org/10.1175/1520-0442(2001)014<1112:GPATFP>2.0.CO;2.

Dai, A. G., K. E. Trenberth, and T. R. Karl, 1999: Effects of clouds, soil moisture, precipitation, and water vapor on diurnal temperature range. *J. Climate*, **12**, 2451–2473, https://doi.org/10.1175/1520-0442(1999)012<2451:EOCSMP>2.0.CO;2.

Dai, A. G., X. Lin, and K. L. Hsu, 2007: The frequency, intensity, and diurnal cycle of precipitation in surface and satellite observations over low- and mid-latitudes. *Climate Dyn.*, **29**, 727–744, https://doi.org/10.1007/s00382-007-0260-y.

Dee, D. P., and Coauthors, 2011: The ERA-interim reanalysis: Con-

figuration and performance of the data assimilation system. *Quart. J. Roy. Meteor. Soc.*, **137**, 553–597, https://doi.org/10.1002/qj.828.

Ding, Y. H., 1992: Summer monsoon rainfalls in China. *J. Meteor. Soc. Japan*, **70**, 373–396, https://doi.org/10.2151/jmsj1965.70.1B_373.

Ding Y. H., and J. C. L. Chan, 2005: The East Asian summer monsoon: An overview. *Meteorol. Atmos. Phys.*, **89**, 117–142, https://doi.org/10.1007/s00703-005-0125-z.

Fu, Y. F., G. S. Liu, G. X. Wu, R. C. Yu, Y. P. Xu, Y. Wang, R. Li, and Q. Liu, 2006: Tower mast of precipitation over the central Tibetan Plateau summer. *Geophys. Res. Lett.*, **33**, L05802, https://doi.org/10.1029/2005GL024713.

Fu, Y. F., and Coauthors, 2020: Land-surface processes and summer-cloud-precipitation characteristics in the Tibetan Plateau and their effects on downstream weather: A review and perspective. *National Science Review*, **7**, 500–515, https://doi.org/10.1093/nsr/nwz226.

Fujinami, H., S. Nomura, and T. Yasunari, 2005: Characteristics of diurnal variations in convection and precipitation over the southern Tibetan Plateau during summer. *SOLA*, **1**, 49–52, https://doi.org/10.2151/sola.2005-014.

Gao, Y. C., and M. F. Liu, 2013: Evaluation of high-resolution satellite precipitation products using rain gauge observations over the Tibetan Plateau. *Hydrology and Earth System Sciences*, **17**, 837–849, https://doi.org/10.5194/hess-17-837-2013.

Ge, J., Q. L. You, and Y. Q. Zhang, 2019: Effect of Tibetan Plateau heating on summer extreme precipitation in eastern China. *Atmos. Res.*, **218**, 364–371, https://doi.org/10.1016/j.atmosres.2018.12.018.

Grabowski, W. W., X. Q. Wu, and M. W. Moncrieff, 1996: Cloud-resolving modeling of tropical cloud systems during phase III of GATE. Part I: Two-dimensional experiments. *J. Atmos. Sci.*, **53**, 3684–3709, https://doi.org/10.1175/1520-0469(1996)053<3684:CRMOTC>2.0.CO;2.

Grabowski, W. W., X. Q. Wu, M. W. Moncrieff, and W. D. Hall, 1998: Cloud-resolving modeling of cloud systems during phase III of GATE. Part II: Effects of resolution and the third spatial dimension. *J. Atmos. Sci.*, **55**, 3264–3282, https://doi.org/10.1175/1520-0469(1998)055<3264:CRMOCS>2.0.CO;2.

Huang, W. R., and J. C. L. Chan, 2012: Seasonal variation of diurnal and semidiurnal rainfall over Southeast China. *Climate Dyn.*, **39**, 1913–1927, https://doi.org/10.1007/s00382-011-1236-5.

Kessler, E., 1969: *On the Distribution and Continuity of Water Substance in Atmospheric Circulations*. American Meteorological Society, 84 pp, https://doi.org/10.1007/978-1-935704-36-2.

Koenig, L. R., and F. W. Murray, 1976: Ice-bearing cumulus cloud evolution: Numerical simulation and general comparison against observations. *J. Appl. Meteorol. Climatol.*, **15**, 747–762, https://doi.org/10.1175/1520-0450(1976)015<0747:IBCCEN>2.0.CO;2.

Li, J., 2018: Hourly station-based precipitation characteristics over the Tibetan Plateau. *International Journal of Climatology*, **38**, 1560–1570, https://doi.org/10.1002/joc.5281.

Li, J., Chen, J., Lu, C., and Wu, X, 2020a: Impacts of TIPEX-III rawinsondes on the dynamics and thermodynamics over the Eastern Tibetan Plateau in the boreal summer. *J. Geophys. Res.: Atmos.*, **125**, e2020JD032635, https://doi.org/10.1029/2020JD032635.

Li, P. X., K. Furtado, T. J. Zhou, H. M. Chen, J. Li, Z. Guo, and C. Xiao, 2020b: The diurnal cycle of East Asian summer monsoon precipitation simulated by the Met Office Unified Model at convection-permitting scales. *Climate Dyn.*, **55**, 131–151, https://doi.org/10.1007/s00382-018-4368-z.

Li, Y. Y., and M. H. Zhang, 2016: Cumulus over the Tibetan Plateau in the summer based on *CloudSat-CALIPSO* data. *J. Climate*, **29**, 1219–1230, https://doi.org/10.1175/JCLI-D-15-0492.1.

Li, Y. Y., and M. H. Zhang, 2017: The role of shallow convection over the Tibetan Plateau. *J. Climate*, **30**, 5791–5803, https://doi.org/10.1175/JCLI-D-16-0599.1.

Li, Y. Y., R. C. Yu, Y. P. Xu, and X. H. Zhang, 2004: Spatial distribution and seasonal variation of cloud over China based on ISCCP data and surface observations. *J. Meteor. Soc. Japan*, **82**, 761–773, https://doi.org/10.2151/jmsj.2004.761.

Liu, W. T., K. B. Katsaros, and J. A. Businger, 1979: Bulk parameterization of air-sea exchanges of heat and water vapor including the molecular constraints at the interface. *J. Atmos. Sci.*, **36**, 1722–1735, https://doi.org/10.1175/1520-0469(1979)036<1722:BPOASE>2.0.CO;2.

Luo, H. B., and M. Yanai, 1983: The large-scale circulation and heat sources over the Tibetan Plateau and surrounding areas during the early summer of 1979. Part I: Precipitation and kinematic analyses. *Mon. Wea. Rev.*, **111**, 922–944, https://doi.org/10.1175/1520-0493(1983)111<0922:TLSCAH>2.0.CO;2.

Luo, H. B., and M. Yanai, 1984: The large-scale circulation and heat sources over the Tibetan Plateau and surrounding areas during the early summer of 1979. Part II: Heat and moisture budgets. *Mon. Wea. Rev.*, **112**, 966–989, https://doi.org/10.1175/1520-0493(1984)112<0966:TLSCAH>2.0.CO;2.

Qie, X. S., X. K. Wu, T. Yuan, J. C. Bian, and D. R. Lu, 2014: Comprehensive pattern of deep convective systems over the Tibetan Plateau-South Asian monsoon region based on TRMM data. *J. Climate*, **27**, 6612–6626, https://doi.org/10.1175/JCLI-D-14-00076.1.

Singh, P., and K. Nakamura, 2009: Diurnal variation in summer precipitation over the central Tibetan Plateau. *J. Geophys. Res.*, **114**, D20107, https://doi.org/10.1029/2009JD011788.

Tao, S., and L. Chen, 1987: A review of recent research on the East Asian summer monsoon in China. *Monsoon Meteorology*, C. P. Chang and T. N. Krishnamurti, Eds., Oxford University Press, 60–92.

Wang, M. R., J. Wang, A. M. Duan, J. Yang, and Y. M. Liu, 2019: Quasi-biweekly impact of the atmospheric heat source over the Tibetan Plateau on summer rainfall in Eastern China. *Climate Dyn.*, **53**, 4489–4504, https://doi.org/10.1007/s00382-019-04798-x.

Wang, X. C., and M. H. Zhang, 2014: Vertical velocity in shallow convection for different plume types. *Journal of Advances in Modeling Earth Systems*, **6**, 478–489, https://doi.org/10.1002/2014MS000318.

Wu, G. X., Y. M. Liu, B. He, Q. Bao, A. M. Duan, and F. F. Jin, 2012: Thermal controls on the Asian summer monsoon. *Scientific Reports*, **2**, 404, https://doi.org/10.1038/srep00404.

Wu, G. X., A. M. Duan, and Y. M. Liu, 2019: Atmospheric heating source over the Tibetan Plateau and its regional climate impact. *Climate Science*. https://doi.org/10.1093/acrefore/9780190228620.013.588.

Wu, J., and X. J. Gao, 2013: A gridded daily observation dataset

over China region and comparison with the other datasets. *Chinese Journal of Geophysics*, **56**, 1102–1111, https://doi.org/10.6038/cjg20130406. (in Chinese with English abstract)

Wu, X. Q., and S. Guimond, 2006: Two- and three-dimensional cloud-resolving model simulations of the mesoscale enhancement of surface heat fluxes by precipitating deep convection. *J. Climate*, **19**, 139–149, https://doi.org/10.1175/JCLI3610.1.

Wu, X. Q., W. W. Grabowski, and M. W. Moncrieff, 1998: Long-term behavior of cloud systems in TOGA COARE and their interactions with radiative and surface processes. Part I: Two-dimensional modeling study. *J. Atmos. Sci.*, **55**, 2693–2714, https://doi.org/10.1175/1520-0469(1998)055<2693:LTBOCS>2.0.CO;2.

Wu, X. Q., W. D. Hall, W. W. Grabowski, M. W. Moncrieff, W. D. Collins, and J. T. Kiehl, 1999: Long-term behavior of cloud systems in TOGA COARE and their interactions with radiative and surface processes. Part II: Effects of ice microphysics on cloud-radiation interaction. *J. Atmos. Sci.*, **56**, 3177–3195, https://doi.org/10.1175/1520-0469(1999)056<3177:LTBOCS>2.0.CO;2.

Wu, X. Q., X. Z. Liang, and S. Park, 2007: Cloud-resolving model simulations over the ARM SGP. *Mon. Wea. Rev.*, **135**, 2841–2853, https://doi.org/10.1175/MWR3438.1.

Xu, W. X., and E. J. Zipser, 2011: Diurnal variations of precipitation, deep convection, and lightning over and east of the Eastern Tibetan Plateau. *J. Climate*, **24**, 448–465, https://doi.org/10.1175/2010JCLI3719.1.

Yanai, M., and T. Tomita, 1998: Seasonal and interannual variability of atmospheric heat sources and moisture sinks as determined from NCEP-NCAR reanalysis. *J. Climate*, **11**, 463–482, https://doi.org/10.1175/1520-0442(1998)011<0463:SAIVOA>2.0.CO;2.

Yanai, M., S. Esbensen, and J. H. Chu, 1973: Determination of bulk properties of tropical cloud clusters from large-scale heat and moisture budgets. *J. Atmos. Sci.*, **30**, 611–627, https://doi.org/10.1175/1520-0469(1973)030<0611:DOBPOT>2.0.CO;2.

Yang, K., T. Koike, H. Fujii, T. Tamura, X. D. Xu, L. E. Bian, and M. Y. Zhou, 2004: The daytime evolution of the atmospheric boundary layer and convection over the Tibetan Plateau: Observations and simulations. *J. Meteor. Soc. Japan*, **82**, 1777–1792, https://doi.org/10.2151/jmsj.82.1777.

Yu, R. C., Y. P. Xu, T. J. Zhou, and J. Li, 2007: Relation between rainfall duration and diurnal variation in the warm season precipitation over central eastern China. *Geophys. Res. Lett.*, **34**, L13703, https://doi.org/10.1029/2007GL030315.

Zhang, C., Q. H. Tang, and D. L. Chen, 2017: Recent changes in the moisture source of precipitation over the Tibetan Plateau. *J. Climate*, **30**, 1807–1819, https://doi.org/10.1175/JCLI-D-15-0842.1.

Zhao, P., and L. X. Chen, 2001: Interannual variability of atmospheric heat source/sink over the Qinghai—Xizang (Tibetan) Plateau and its relation to circulation. *Adv. Atmos. Sci.*, **18**, 106–116, https://doi.org/10.1007/s00376-001-0007-3.

Zhou, T. J., R. C. Yu, H. M. Chen, A. G. Dai, and Y. Pan, 2008: Summer precipitation frequency, intensity, and diurnal cycle over China: A comparison of satellite data with rain gauge observations. *J. Climate*, **21**, 3997–4010, https://doi.org/10.1175/2008JCLI2028.1.